Petroleum Science 20 (2023) 241–248

Contents lists available at ScienceDirect

Petroleum Science

journal homepage: www.keaipublishing.com/en/journals/petroleum-science

Original Paper

A nonparametric spectrum estimation method for dispersion and attenuation analysis of borehole acoustic measurements

Bing Wang [a, *], Wei Li [b], Qing Ye [a], Kun-Yu Ma [a]

[a] State Key Laboratory of Petroleum Resources and Prospecting, China University of Petroleum, Beijing, 102249, China
[b] Beijing Research Center, Aramco Asia, Beijing, 100102, China

ARTICLE INFO

Article history:
Received 15 February 2022
Received in revised form
21 April 2022
Accepted 15 September 2022
Available online 21 September 2022

Edited by Jie Hao

Keywords:
Dispersion analysis
Attenuation factor
Nonparametric spectrum estimation method
Acoustic logging
Fluid type evaluation

ABSTRACT

Dispersion and attenuation analysis can be used to determine formation anisotropy induced by fractures, or stresses. In this paper, we propose a nonparametric spectrum estimation method to get phase dispersion characteristics and attenuation coefficient. By designing an appropriate vector filter, phase velocity, attenuation coefficient and amplitude can be inverted from the waveform recorded by the receiver array. Performance analysis of this algorithm is compared with Extended Prony Method (EPM) and Forward and Backward Matrix Pencil (FBMP) method. Based on the analysis results, the proposed method is capable of achieving high resolution and precision as the parametric spectrum estimation methods. At the meantime, it also keeps high stability as the other nonparametric spectrum estimation methods. At last, applications to synthetic waveforms modeled using finite difference method and real data show its efficiency. The real data processing results show that the P-wave attenuation log is more sensitive to oil formation compared to S-wave; and the S-wave attenuation log is more sensitive to shale formation compared to P-wave.

1. Introduction

Method of dispersion and attenuation analysis has attracted an increasing attention in geophysical signal processing, especially in borehole acoustic measurements. Dispersion characteristics of borehole acoustic modes such as Stoneley mode of monopole source and flexural mode of dipole source are widely used to invert the velocity of the borehole wall formation and radial shear velocity profile of the formation (Burridge and Sinha, 1996; Tang and Douglas, 2010; Wang et al., 2017; Fang and Cheng, 2017; Wang and Zhang, 2018; Lebedev, 2021). Dispersion property of cross-dipole measurement can be used to determine formation anisotropy induced by fractures or stresses (Li et al. 2016, 2020).

Numerous algorithms have been introduced into borehole acoustic dispersion analysis. These methods can be divided into two types: model-based and data-driven. For the model-based methods, the acoustic waveform is considered to be a summation of a specific number of propagation modes. By defining the propagation parameters for each mode, the dispersion characteristic can be solved from the waveform array. Theses parametric methods include Prony method, ESPRIT, matrix pencil (MP) (Li et al., 2015), and extended versions of the above (Zeng et al., 2018; Chen et al., 2020). These algorithms have good accuracy results while requiring prior knowledge of the exact number of wave modes propagated in the signal. Due to this limitation, some data-driven methods are proposed such as modified maximum-likelihood (MML) method, weighted spectral semblance (WSS) and amplitude and phase estimation (APES) method (Li et al., 2015). Based on a coherence maximization technique, WSS method can only identify the strongest mode at a given frequency when multiple modes. MML method is equivalent to the minimum variance distortionless response method (CAPON method). By using short-time Fourier transform and a normalization technique, this method can identify separate similar arrivals with heavy computational cost (Wathelet et al., 2018; Zeng et al., 2021). A phase-based dispersion analysis method is proposed to calculate the dispersion curve directly (Assous et al., 2014). The phase velocity of wave mode in every frequency can be calculated using the phase slope after unwrapping. Its fast processing time and high accuracy make it efficient in industry application. For these two parametric and nonparametric dispersion methods, the phase dispersion of the mode wave can be

* Corresponding author.
E-mail address: wangbing@cup.edu.cn (B. Wang).

https://doi.org/10.1016/j.petsci.2022.09.011

estimated within reasonable accuracy. Besides the phase velocity of the wave mode, the attenuation information in acoustic logging measurements can help evaluate formation effectively. The attenuation characteristics of the propagation waveforms can help us understand the property of the formation which has promising application in shale gas formation evaluation (Pan et al., 2017; Yang et al., 2019; Zhuang et al., 2019). But all these dispersion analysis methods mentioned above cannot get the attenuation estimation directly.

In this paper, a nonparametric spectrum estimation method is proposed to get phase dispersion characteristics and attenuation coefficient. By designing an appropriate vector filter, phase velocity, attenuation coefficient and amplitude can be inverted from the waveform recorded by the receiver array. Performance analysis of this algorithm is carried out through theoretical computation. In order to investigate the stability of the algorithm, random noises with different noise to signal ratios are introduced and reasonable results are thus obtained. At last, application to synthetic waveforms modeled using finite-difference method and real data shows its efficiency.

2. Nonparametric methods for frequency dispersion and attenuation estimation

Suppose a signal sequence $x(n)$ in space domain is superimposed by p complex sinusoidal signal sequences with additive noise,

$$x(n)=\sum_{k=1}^{p}\alpha_k e^{-(\rho_k+iws_k)d(n-1)}+v(n),\ n=1,\ldots\ldots,N \tag{1}$$

where ρ_k, s_k and α_k are the attenuation factor, slowness and amplitude of the kth mode with respect to frequency ω, $v(n)$ is noise signal. Then an FIR filter $\boldsymbol{w}$ with a length of M is designed and applied into $\boldsymbol{x}(n)$, the output $y(n)$ is

$$y(n)=\boldsymbol{w}^H\boldsymbol{x}(n)=\boldsymbol{x}^H(n)\boldsymbol{w} \tag{2}$$

in which, $\boldsymbol{x}(n)=[x(n),\ x(n+1),\ \ldots,\ x(n+M-1)]^{\mathrm{T}}$ denotes the backward filtering vector, $\boldsymbol{w}=[w_1,\ w_2,\ \ldots,\ w_M]^{\mathrm{T}}$ denotes weighting coefficient vector of this filter. According to Eq. (1), the signal sequence $\boldsymbol{x}(n)$ can be written as matrix form:

$$\boldsymbol{x}(n)=\boldsymbol{A}\boldsymbol{s}(n)+\boldsymbol{v}(n)\in C^{M\times 1} \tag{3}$$

where, $\boldsymbol{s}$ is signal vector, $\boldsymbol{A}$ is the direction vector of the signal and $\boldsymbol{v}$ is noise vector, which are expressed as

$$\boldsymbol{A}=\begin{bmatrix}\boldsymbol{a}(\rho_1,s_1)\\ \boldsymbol{a}(\rho_2,s_2)\\ \vdots\\ \boldsymbol{a}(\rho_p,s_p)\end{bmatrix}^{\mathrm{T}},\boldsymbol{s}(n)=\begin{bmatrix}\alpha_1 e^{-(\rho_1+iws_1)(n-1)d}\\ \alpha_2 e^{-(\rho_2+iws_2)(n-1)d}\\ \vdots\\ \alpha_p e^{-(\rho_p+iws_p)(n-1)d}\end{bmatrix},\boldsymbol{v}(n)=\begin{bmatrix}v(n)\\ v(n+1)\\ \vdots\\ v(n+M-1)\end{bmatrix} \tag{4}$$

where, $\boldsymbol{a}(\rho,s)=\begin{bmatrix}1 & e^{-(\rho+iws)d} & \ldots & e^{-(\rho+iws)(M-1)d}\end{bmatrix}^{\mathrm{T}}$. The output can thus be expressed as

$$\boldsymbol{w}^H\boldsymbol{x}(n)=\boldsymbol{w}^H\left[\boldsymbol{a}(\rho_1,s_1)\alpha_1 e^{-(\rho_1+iws_1)(n-1)d}+\sum_{k=2}^{p}\boldsymbol{a}(\rho_k,s_k)\alpha_k e^{-(\rho_k+iws_k)(n-1)d}+\boldsymbol{v}(n)\right] \tag{5}$$

When the constraints (2D CAPON method) of this filter are

1) The filter passes through a decayed sine signal (the signal's parameter is (α,ρ,s)) without distortion.
2) The total output power of this filter is the minimum.

The design of the filter can be considered as optimization problem

$$\min_{\boldsymbol{w}}\frac{1}{L}E\left\{\left|\boldsymbol{w}^H\boldsymbol{x}(n)\right|^2\right\}\quad s.t.\quad \boldsymbol{w}^H\boldsymbol{a}(\rho,s)=1 \tag{6}$$

Let the covariance matrix $\boldsymbol{R}$ be the power of the filter, the above equation can be rewritten as

$$\min_{\boldsymbol{w}}\boldsymbol{w}^H\hat{\boldsymbol{R}}\boldsymbol{w}\quad s.t.\quad \boldsymbol{w}^H\boldsymbol{a}(\rho,s)=1 \tag{7}$$

in which, $\hat{\boldsymbol{R}}=\frac{1}{L}\sum_{n=1}^{L}\boldsymbol{x}(n)\boldsymbol{x}^H(n)$ is the approximation of covariance matrix $\boldsymbol{R}$, $L=N-M+1$. According to Lagrange multiplier method, the weighting vector of this filter, or the solution of the constraint optimization problem is

$$\hat{\boldsymbol{w}}_{\mathrm{CAPON2D}}(\rho,s)=\frac{\hat{\boldsymbol{R}}^{-1}\boldsymbol{a}(\rho,s)}{\boldsymbol{a}^H(\rho,s)\hat{\boldsymbol{R}}^{-1}\boldsymbol{a}(\rho,s)} \tag{8}$$

Given the presence of an attenuated sinusoidal signal component with its parameter of (α,ρ,s), the output of Eq. (8) is

$$\hat{\boldsymbol{w}}^H{}_{\mathrm{CAPON2D}}(\rho,s)\boldsymbol{x}(n)=\alpha e^{-(\rho+iws)(n-1)d}+e_F(n) \tag{9}$$

where, $n=1,2,\ldots,N$, $e_F(n)$ is the filter output of noise and all other sinusoidal signal components. For a given (ρ, s), the least square estimation of the complex amplitude α is

$$\hat{\alpha}_{CAPON2D}(\rho,s)=\frac{1}{L_p(\rho)}\frac{\boldsymbol{a}^H(\rho,s)\hat{\boldsymbol{R}}^{-1}\boldsymbol{g}(\rho,s)}{\boldsymbol{a}^H(\rho,s)\hat{\boldsymbol{R}}^{-1}\boldsymbol{a}(\rho,s)} \tag{10}$$

$L_p=\frac{1-e^{-2\rho dL}}{L(1-e^{-2\rho d})}$, and $L_p=1.0$ when $\rho=0$; $\boldsymbol{g}(\rho,s)=\frac{1}{L}\sum_{n=1}^{L}\boldsymbol{x}(n)e^{(iws-\rho)(n-1)d}$

The estimation of filter weighting vector and amplitude spectrum in Eqs. (9) and (10) is based on the 2D extension of 1D CAPON method (1D means slowness dimension, 2D means slowness and attenuation dimension), we call it CAPON2D in this paper.

When the constraints (2D APES method) of the filter are:

1) The filter passes through a decayed sine signal (the signal's parameter is (α,ρ,s) without distortion.
2) The total output power with respect to all the other sinusoidal signal components and noise of this filter is the minimum.

The design of the filter can be considered as an optimization problem

$$\min_{\boldsymbol{w},\alpha}\left\{J(\boldsymbol{w},\alpha)=^{\Delta}\frac{1}{L}\sum_{n=1}^{L}\left|\boldsymbol{w}^H\boldsymbol{x}(n)-\alpha e^{-(\rho+ws)(n-1)d}\right|^2\right\}\ s.t.\ \boldsymbol{w}^H\boldsymbol{a}(\rho,s)=1 \tag{11}$$

Expand the objective function $J(\boldsymbol{w}, \alpha)$ in Eq. (11) as

$$\begin{aligned}J(\boldsymbol{w},\alpha)&=\boldsymbol{w}^H\widehat{\boldsymbol{R}}\boldsymbol{w}-\alpha^*\boldsymbol{w}^H\boldsymbol{g}(\rho,s)-\alpha\boldsymbol{g}^H(\rho,s)\boldsymbol{w}+|\alpha|^2L_p\\&=L_p\left|\alpha-\frac{1}{L_p}\boldsymbol{w}^H\boldsymbol{g}(\rho,s)\right|^2+\boldsymbol{w}^H\left[\widehat{\boldsymbol{R}}-\boldsymbol{g}_1(\rho,s)\boldsymbol{g}_1{}^H(\rho,s)\right]\boldsymbol{w}\end{aligned} \tag{12}$$

where,

$$\widehat{\boldsymbol{R}}=\frac{1}{L}\sum_{n=1}^{L}\boldsymbol{x}(n)\boldsymbol{x}^H(n) \tag{13}$$

$$\boldsymbol{g}(\rho,s)=\frac{1}{L}\sum_{n=1}^{L}\boldsymbol{x}(n)e^{(iws-\rho)(n-1)d},\ \boldsymbol{g}_1(\rho,s)=\frac{1}{\sqrt{L_p}}\boldsymbol{g}(\rho,s) \tag{14}$$

$$L_p=\frac{1}{L}\sum_{n=1}^{L}e^{-2\rho d(n-1)}=\frac{1-e^{-2\rho dL}}{L\left(1-e^{-2\rho d}\right)} \tag{15}$$

In order to minimize the objective function $J(w, \alpha)$, we have

$$\alpha=\frac{1}{L_p}\boldsymbol{w}^H\boldsymbol{g}(\rho,s) \tag{16}$$

The optimization objective function in Eq. (11) can be expressed as:

$$J(\boldsymbol{w},\alpha)=\boldsymbol{w}^H\hat{\boldsymbol{Q}}\boldsymbol{w}\ \ s.t.\ \ \boldsymbol{w}^H\boldsymbol{a}(\rho,s)=1 \tag{17}$$

Based on the Lagrange multiplier method and Eq. (16), the solution of Eq. (17) can be expressed as:

$$\widehat{\mathbf{w}}_{\mathrm{APES2D}}(\rho,s)=\frac{\widehat{\boldsymbol{Q}}^{-1}\boldsymbol{a}(\rho,s)}{\boldsymbol{a}^H(\rho,s)\widehat{\boldsymbol{Q}}^{-1}\boldsymbol{a}(\rho,s)} \tag{18}$$

$$\widehat{\boldsymbol{\alpha}}_{\mathrm{APES2D}}(\rho,s)=\frac{1}{L_p(\rho)}\frac{\boldsymbol{a}^H(\rho,s)\widehat{\boldsymbol{Q}}^{-1}\boldsymbol{g}(\rho,s)}{\boldsymbol{a}^H(\rho,s)\widehat{\boldsymbol{Q}}^{-1}\boldsymbol{a}(\rho,s)} \tag{19}$$

where, $\widehat{\boldsymbol{Q}}(\rho,s)=\widehat{\boldsymbol{R}}-\boldsymbol{g}(\rho,s)\boldsymbol{g}^H(\rho,s)$ is the estimation of the noise covariance matrix.

The estimation of filter weighting vector and amplitude spectrum in Eqs. (18) and (19) is based on the 2D extension of 1D APES method, we call it APES2D in this paper.

Based on the above discussion, the procedures of adaptive filtering high resolution evaluation of dispersion and attenuation are:

Step 1: Fourier transform of the time domain signal to get its frequency spectrum $X(n)$;
Step 2: Given a frequency ω, calculate the estimation of covariance matrix $\boldsymbol{R}$ based on Eq. (7);
Step 3: Scan slowness s and attenuation ρ in a given range, apply CAPON2D and APES2D method based on Eqs. (10) and (19) to estimate amplitude spectrum, find the corresponding locations of the peak values in slowness-attenuation plane, and get the estimation of slowness and attenuation for different modes (more than one peak value may be present).
Step 4: Scan the signal frequency in the effective frequency band to get the estimation of slowness and attenuation for different modes.

3. Performance analysis

To test the statistical performance of the adaptive filtering dispersion and attenuation estimation method (AFDAES), we build a set of complex signal sequence based on the damped complex sinusoidal signal superposition model. And evaluate the performance of AFDAES by analyzing the estimation results of slowness, attenuation and amplitude when applying the AFDAES to the pure model signal as well as the signals with different degrees of white noise.

In this test, the model is defined as

$$x(n)=\sum_{k=1}^{p}\alpha_k e^{-(\rho_k+iws_k)(n-1)d}+v(n),\ n=1,\ \ldots,\ N \tag{20}$$

in which, the model parameters are designed according to the real acoustic logging data, the details are shown in Table 1.

Based on Eq.(17) and the parameters in Table 1, the real and imaginary part of the damped complex signal are shown in Fig. 1.

First, the 2D CAPON method is applied to estimate the slowness and attenuation of the original model data in Fig. 1. In Fig. 2, the true amplitude of original data is labeled in red "*". To highlight the locations of the peak values, the amplitude axis in Fig. 2 is the logarithm of the estimate calculated using 2D CAPON method. Four peak values are present in Fig. 2, and there is only one peak value for each fixed slowness. Therefore, in order to find the peak values in 2D amplitude spectrum $\alpha(\rho, s)$, we have to 1) select the attenuation value ρ_i that assures the amplitude reaches the maximum for each slowness s_i, obtain the 1D amplitude spectrum $\alpha(s)$ that changes with slowness (blue lines in Fig. 3) and the corresponding attenuation $\rho(s)$; and 2) find the slowness s_k with respect to the maximum α in the 1D amplitude spectrum $\alpha(s)$ in Fig. 3 and the attenuation ρ corresponding to the slowness s_i. The slowness and attenuation estimation of the four sinusoidal signal components in $x(n)$ are thus obtained with $\boldsymbol{s}$ = [80; 120; 160; 200],$\boldsymbol{\rho}$ = [0.2; 0.3; 0.5; 0.1]; 3) based on the estimated slowness and attenuation, estimate the amplitude $\boldsymbol{\alpha}$ of the sinusoidal signal components using 2D APES method (Eq. (19)), $\boldsymbol{\alpha}=[4+i;\ 1-i;\ 3-i;\ 2+i]$. For original signals without noise, the estimation of slowness and attenuation works perfect without any error when applying the adaptive filtering method.

For comparison, estimation results (slowness, attenuation and amplitude) of the original signal using AFDAES, extended Prony method (EPM) and modified Matrix Pencil method (FBMP) are shown in Table 2. Positive error in Table 2 means estimated value is larger than the true value, and vice versa, 0 means estimated value

Table 1
Parameters for the complex weighted damped exponential model.

Name	Symbol	Unit	Value
Sample number	N	–	13
Sample interval	D	ft	0.5
Central frequency	ω_0	kHz	8
Mode number	P	–	4
Complex coefficient	B	–	$[4+i;\ 2-i;\ 3-i;\ 1+i]$
Slowness	S	us/ft	[80; 120; 160; 200]
Attenuation coefficient	P	–	[0.2; 0.3; 0.5; 0.1]

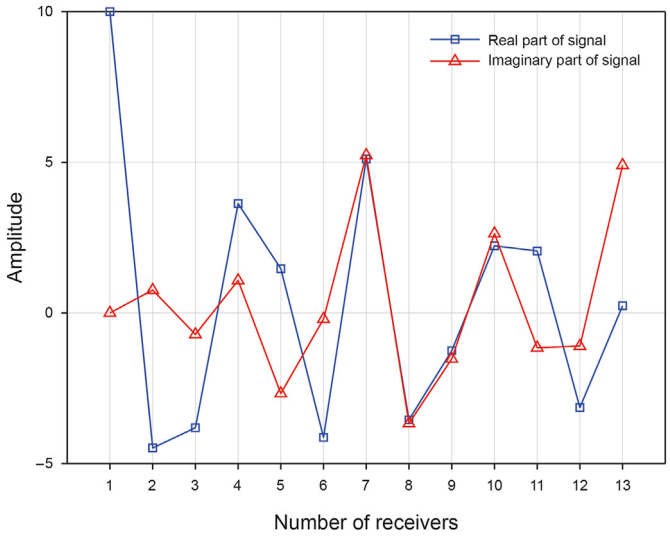

Fig. 1. Spatial damped complex exponential signal.

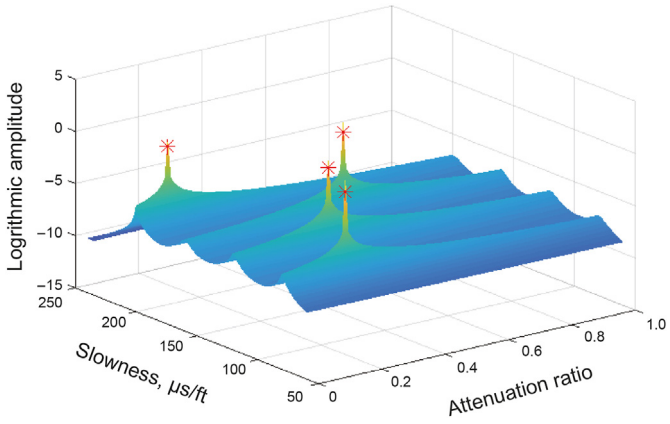

Fig. 2. 2D amplitude spectra α(ρ, s) from 2D CAPON method.

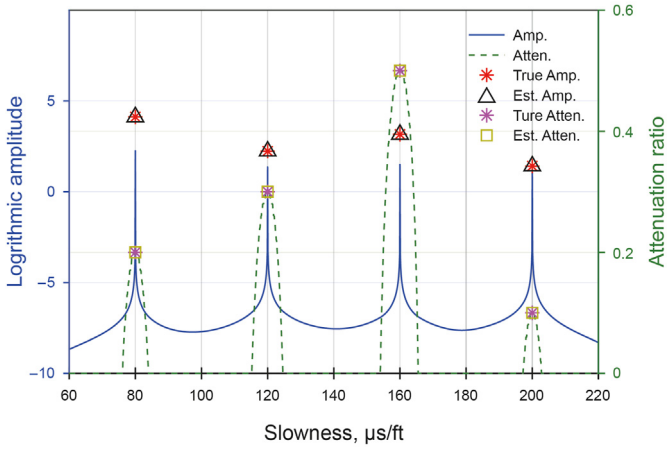

Fig. 3. 1D amplitude spectra α(s) (blue line) and attenuation ρ(s) (green dash).

equals to the true value.

From Table 2, both of the AFDAES method based on the nonparametric spectrum estimation and the FBMP method based on the parametric spectrum estimation can achieve precise estimation of slowness, attenuation and amplitude of the sinusoidal signal components in the original noise-free signal, however, some degree of error occurs when the EPM method is applied. This implies the AFDAES method, as a nonparametric spectrum estimation method, is superior to the optimum parametric spectrum estimation method, which in the meantime, avoids the disadvantage of the parametric spectrum estimation method (the number of sinusoidal signal components in the model must be known).

Now, let's consider situations when noise is present in the model signal. By applying 100 times of Monte Carlo simulations to the original model signal in Fig. 1 when signal to noise ration $S/N = 25$ dB, the estimation results of the slowness, attenuation and amplitude for the four sinusoidal signal components are shown in Fig. 4. In this figure, the true parameters of original data is labeled in red "*" and the blue ones are the estimated values when different methods are applied. The comparison results of the three methods in Fig. 4 show that, all the three methods can achieve satisfying estimation of the slowness, whereas, the projections of the estimated values obtained by AFDAES and FBMP on the slowness axis are smaller than that obtained by the EPM method. Compared with the other two methods, the EPM method is slightly poorer in slowness estimation. For the estimation of attenuation and amplitude, the EPM results are not that satisfying compared with the other two methods. Both the AFDAES and FBMP method provide fairly precise results, while the AFDAES has a superior stability (the smaller the projection area, the smaller the variance is, and the more stable the method is).

Based on the above analysis, the AFDAES, as a nonparametric spectrum estimation method, is capable of achieving high resolution and precision as the parametric spectrum estimation methods in the meantime, it also keeps high stability as the other nonparametric spectrum estimation methods.

4. Processing on numerical simulation waveforms

In order to investigate the efficiency of the algorithm, we apply this method to synthetic waveforms simulated with FD. The simulation model is shown in Fig. 5, in which the borehole radius is 0.127 m, compressional velocity of borehole fluid is 1500 m/s and the fluid density is 1000 kg/m^3. The compressional and shear velocity of the formation outside the borehole is shown in Fig. 5. The new proposed AFDAES method will be applied into this model.

4.1. Results on monopole data

Different source types can trigger very different wave fields in the borehole. Monopole and dipole sources are commonly used types in acoustic logging. First, the monopole source is used in the simulation. The distance between the source and the receiver array is from 2.74 m (9 ft) to 4.72 m (15.5 ft). The 13 receivers are evenly spaced with an interval of 0.1524 m (0.5 ft). The finite difference method is applied to simulate the monopole waveforms with a central frequency of 9 kHz. The simulated waveforms and spectrums are shown in Fig. 6. We can see that the Stoneley wave is the strongest component in the waveforms with a relative lower frequency. Refracted compressional and shear wave have small amplitudes. And different velocities can be identified from the different slopes for different components.

Fig. 7 shows the dispersion (Fig. 7a) and attenuation (Fig. 7b) results processed with new proposed AFDAES method. The back dots in Fig. 7a stand for the theoretical dispersion curves showing

Table 2
Errors of the estimated parameters from pure signal by AFDAES, EPM, and FBMP.

Method	Estimated error of s	Estimated error of ρ	Estimated error of $\|b\|$
AFDAES	[0; 0; 0; 0]	[0; 0; 0; 0]	[0; 0; 0; 0]
EPM	[0.05; 0.09; −0.09; −0.20]	[0.01; −0.77; −0.78; 0.67]	[0.68; 0.38; 0.96; 0.13]
FBMP	[0; 0; 0; 0]	[0; 0; 0; 0]	[0; 0; 0; 0]

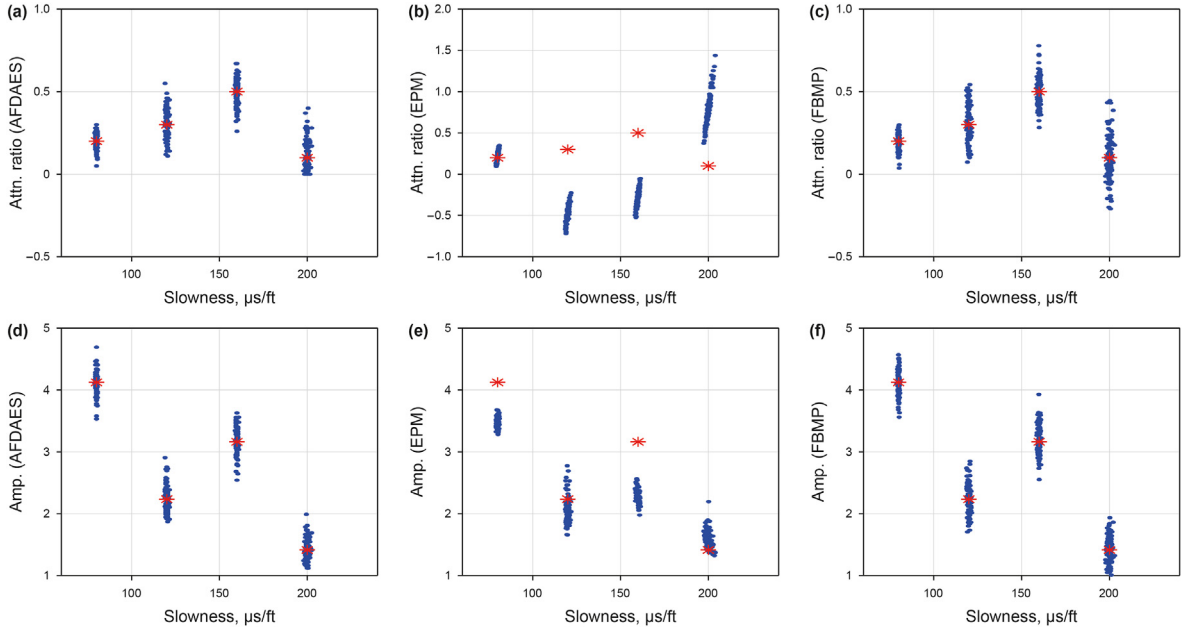

Fig. 4. 100 times Monte Carlo experiments of parameter estimations (blue dots) for 25 dB noisy data using AFDAES, EPM and FBMP methods compared with true values (red star).

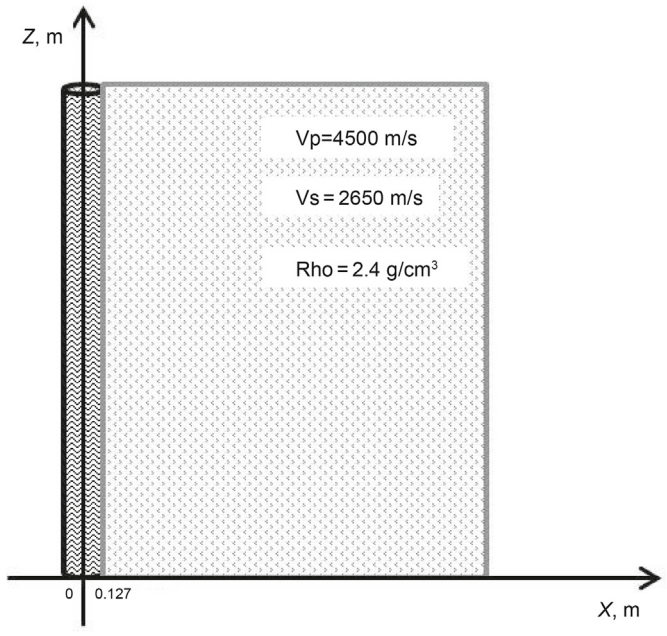

Fig. 5. Geometry of the acoustic well logging model.

here for reference. The refracted compressional and shear wave are non-dispersive, so there are no dispersion characteristics of the two waveform component, as shown in Fig. 7a. Stoneley wave has a slight dispersion and its dispersion is reversed, slowness decreases with frequency increases. As a special tube wave, Stoneley wave propagates along the borehole wall and barely decays in its traveling path. Attenuation result in Fig. 7b (cyan color) shows the attenuation characteristic of Stoneley wave with a very small value. As the formation is a fast formation in acoustic logging, pseudo-Rayleigh wave travels in accompany with Stoneley wave. And its dispersion is strong, which is the reason that we cannot see obvious pattern in the waveforms (Fig. 6). From the dispersion analysis results, different orders of pseudo-Rayleigh wave (pR_1 (red), pR_2 (green) and pR_3 (blue)) can be seen. And the attenuation information can also be identified in Fig. 7b. Besides, from Fig. 7, the slowness and attenuation of different modes change with different frequencies. All the mode waves suffer from severe attenuation at both sides of the frequency band, where the signal energy is the lowest.

4.2. Results on dipole waveforms

Dipole source is then simulated using the same formation parameters with monopole case. The full waveforms simulated by the finite difference method and spectrums are shown in Fig. 8. The dominant energy in dipole waveforms is flexure mode. In Fig. 9, the frequency dispersion curves (Fig. 9a) and the corresponding attenuation coefficients (Fig. 9b) are obtained when AFDAES method is applied. The back dots in Fig. 9a stand for the theoretical dispersion curves showing here for reference. Three kinds of the mode waves are shown in Fig. 9, which are the first order (red), second order (green) and third order (blue) flexural waves. Due to their (second and third order) low amplitude in the waveforms, their attenuation is also very small. The attenuation of the flexural

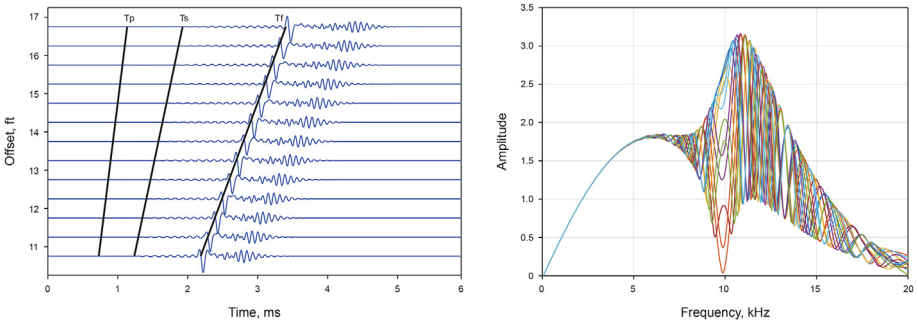

Fig. 6. Full waveforms (left) and spectrum (right) of the model in fast formation with a monopole source.

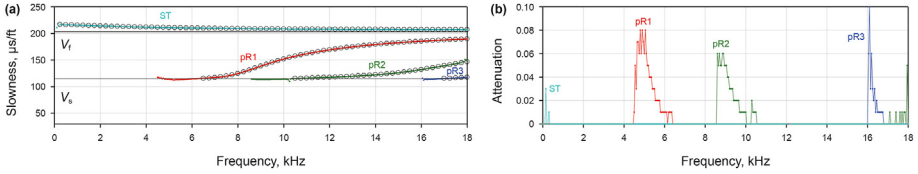

Fig. 7. Fast formation model, monopole source: Slowness (a) and attenuation (b) estimations by AFDAES method.

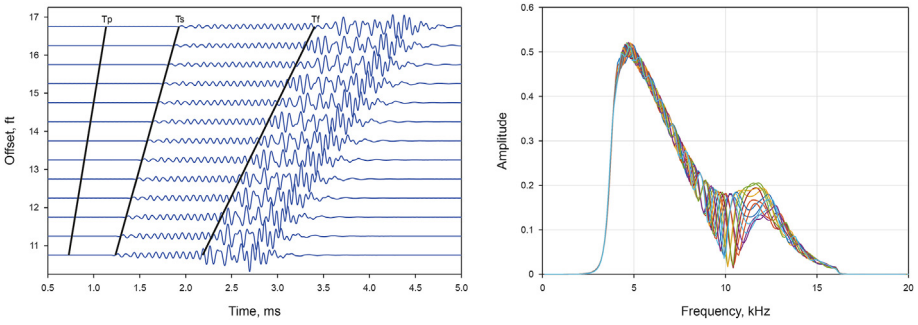

Fig. 8. Fast formation model, dipole source: full waveforms (left), spectrum (right).

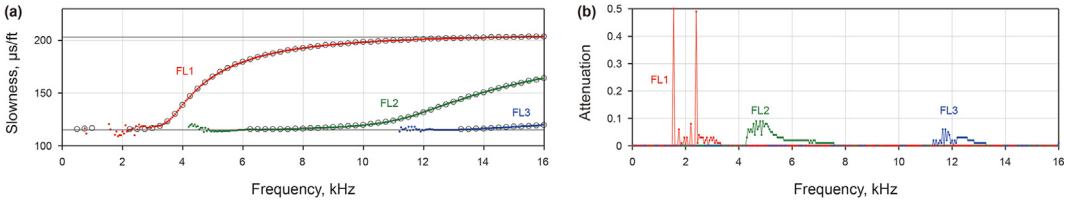

Fig. 9. Parallel boundary, fast formation model, dipole source: slowness (a) and attenuation (b) estimations by AFDAES method.

waves with different orders also occurs at both sides of the frequency band.

5. Processing on real waveforms

There are several factors that can cause waveform attenuation in the borehole. For the acoustic logging measurement, the main factor should be the rock intrinsic attenuation. We can evaluate the fluid type and lithology by the P and S wave attenuation differences. In this section, a real data from western China is processed using AFDAES. As shown in Fig. 10, the first column is the Gamma ray (GR) track. The second track is the depth track. Monopole waveforms are shown in the third track as input data for slowness and attenuation estimation. Travel times (TT) for P- and S-wave are overlaid on top of the waveforms. In the fourth track, it shows the attenuation and amplitude of P- and S-wave obtained by AFDAES, which are the averaged value of the inverted results within the energy dominant frequency band. Track 5 and Track 6 are the porosity (POR) and oil saturation. The last track is the interpretation results. There are two typical sections interpreted. Section I is a shale formation, with high GR, relatively higher attenuation on S-wave, high POR and low oil saturation. Section II is an oil formation, with low GR, relatively higher attenuation on P-wave, moderate POR and high oil saturation. So the results show very much consistency with other logs and

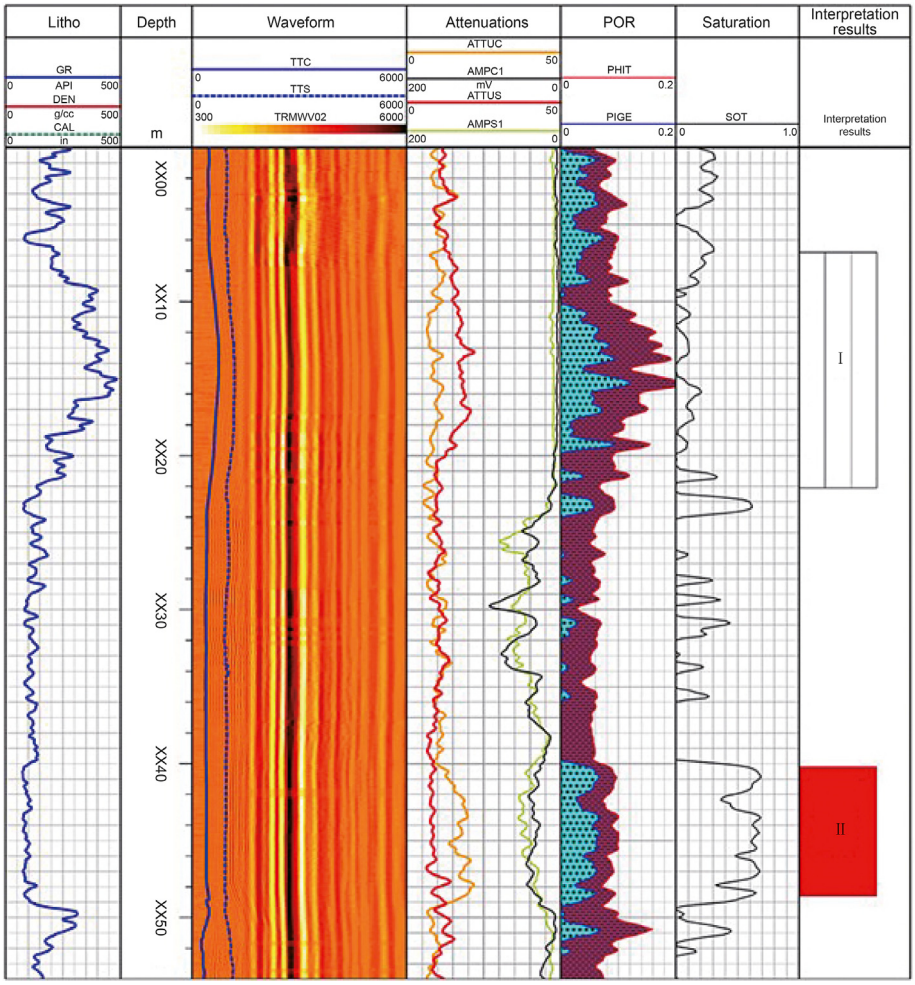

Fig. 10. Attenuation processing results of real data.

indicate that P-wave attenuation log is more sensitive to oil formation compared to S-wave; and S-wave attenuation log is more sensitive to shale formation compared to P-wave.

6. Conclusion

Efficient dispersion and attenuation estimation algorithm can be applied to acoustic well logging to determine formation anisotropy induced by fractures, or stresses. In this paper, the new proposed AFDAES method used to get phase dispersion characteristics and attenuation coefficient. For the performance analysis of this method, the estimation results of slowness, attenuation and amplitude using AFDAES are compared with EPM and FBMP. Based on the analysis, the AFDAES, as a nonparametric spectrum estimation method, is capable of achieving high resolution and precision as the parametric spectrum estimation methods in the meantime, it also keeps high stability as the other nonparametric spectrum estimation methods. Finally, the processing results of numerical waveforms and real data show its validity in waveform characteristics estimation. The real data processing results show that the P-wave attenuation log is more sensitive to oil formation compared to S-wave; and the S-wave attenuation log is more sensitive to shale formation compared to P-wave.

Acknowledgments

This research was supported by the National Natural Science Foundation of China (No. 42274141), Science Foundation of China University of Petroleum, Beijing (No. 2462020YXZZ007).

References

Assous, S., Elkington, P., Linnett, L., 2014. Phase-based dispersion analysis for acoustic array borehole logging data. J. Acoust. Soc. Am. 135 (4), 1919–1928. https://doi.org/10.1121/1.4868396.

Burridge, R., Sinha, B.K., 1996. Inversion for formation shear modulus and radial depth of investigation using borehole flexural waves: SEG Technical Program Expanded Abstracts. https://doi.org/10.1190/1.1826426, 158-161.

Chen, D., Guan, W., Zhang, C., et al., 2020. High-resolution inversion for dispersion characteristics of acoustic logging waveforms. J. Geophys. Eng. 17 (3), 439–450. https://doi.org/10.1093/jge/gxaa003.

Fang, X., Cheng, A., 2017. Detection of formation shear wave in a slow formation using a monopole acoustic logging-while-drilling tool. Geophysics 83 (1), D9–D16. https://doi.org/10.1190/geo2017-0300.1.

Lebedev, A.V., 2021. A way to simplify calculations in acoustic logging. Geophysics 86 (5), 1–22. https://doi.org/10.1190/geo2020-0893.1.

Li, W., Tao, G., Matuszyk, J.P., et al., 2015. Forward and backward amplitude and phase estimation method for dispersion analysis of borehole sonic measurements. Geophysics 80 (3), D295–D308. https://doi.org/10.1190/geo2014-0298.1.

Li, M., Tao, G., Wang, H., et al., 2016. An improved multiscale and leaky P-wave removal analysis for shear-wave anisotropy inversion with crossed-dipole logs. Petrophysics 57 (03), 270–293 https://doi.org/SPWLA-2016-v57n3a4.

Li, Y.H., Xu, S., Jiang, C., et al., 2020. Joint inversion of logging-while-drilling multipole acoustic data to determine formation shear-wave transverse isotropy. Geophysics 85 (4), 1–43. https://doi.org/10.1190/geo2019-0611.1, 2020.

Pan, B.Z., Yuan, M., Fang, C., et al., 2017. Experiments on acoustic measurement of

fractured rocks and application of acoustic logging data to evaluation of fractures. Petrol. Sci. 14, 520–528. https://doi.org/10.1007/S12182-017-0173-2.
Tang, X.M., Douglas, J.P., 2010. Mapping formation radial shear-wave velocity variation by a constrained inversion of borehole flexural-wave dispersion data. Geophysics 75, E183–E190. https://doi.org/10.1190/1.3502664.
Wang, B., Zhang, K., 2018. Direct inversion algorithm for shear velocity profiling in dipole acoustic borehole measurements. Geosci. Rem. Sens. Lett. IEEE 15 (6), 828–832. https://doi.org/10.1109/LGRS.2018.2812857.
Wang, H., Fehler, M.C., Miller, D., 2017. Reliability of velocity measurements made by monopole acoustic logging-while-drilling tools in fast formations. Geophysics 82, D225–D233. https://doi.org/10.1190/geo2016-0387.1.
Wathelet, M., Guillier, B., Roux, P., et al., 2018. Rayleigh wave three-component beamforming: signed ellipticity assessment from high-resolution frequency-wavenumber processing of ambient vibration arrays. Geophys. J. Int. 215 (1), 507–523. https://doi.org/10.1093/gji/ggy286.
Yang, B., Zhang, C., Cai, M., et al., 2019. Research on evaluation method of fracture permeability based on stoneley wave energy attenuation. Prog. Geophys. 34 (03), 1127–1131. https://doi.org/10.6038/pg2019CC0121 (in Chinese).
Zeng, F., Yue, W., Li, C., 2018. Dispersion analysis of borehole sonic measurements by Hilbert transform and band-pass filters. Geophysics 83 (4), D127–D150. https://doi.org/10.1190/geo2017-0580.1.
Zeng, F., Yue, W., Li, C., et al., 2021. Estimation of the transversely isotropic formation parameters using flexural and quadrupole dispersion data in the fast formation. Geophysics 86 (4), 1–70. https://doi.org/10.1190/geo2019-0567.1.
Zhuang, C.X., Yanghu, L., Kong, F., et al., 2019. Formation permeability estimation using Stoneley waves from logging while drilling:theory,method,and application. Chin. J. Geophys. 62 (11), 4482–4492. https://doi.org/10.6038/cjg2019N0122 (in Chinese).